applied optics

Array illumination of a Fresnel–Dammann zone plate

Yayao Ma,[1] Chaochao Ye,[1] Jie Ke,[2,3] Junyong Zhang,[2,*] Jianqiang Zhu,[2] and Zunqing Ling[2]

[1]Huazhong University of Science and Technology, Wuhan 430074, China
[2]National Laboratory on High Power Laser and Physics, Shanghai Institute of Optics and Fine Mechanics, Chinese Academy of Sciences, Shanghai 201800, China
[3]University of Chinese Academy of Science, Beijing 100049, China
*Corresponding author: zhangjin829@163.com

Received 17 May 2016; revised 6 August 2016; accepted 9 August 2016; posted 11 August 2016 (Doc. ID 265331); published 2 September 2016

The traditional Dammann grating is a phase-only modulation, and its theoretical foundation is based on far-field diffraction. Here we extend the traditional Fresnel zone plate (FZP) into a Fresnel–Dammann zone plate (FDZP), which is, in essence, considered as a FZP with Dammann modulation. Different from the Dammann grating, a single FDZP can generate array illumination from the near field to the far field by means of amplitude-only modulation in the absence of phase modulation. We then give some array illuminations operated in a water window to validate the feasibility and validity. This kind of wave-front modulation technology can be applied to array focusing and imaging from the x-ray to the EUV region.

OCIS codes: (050.1950) Diffraction gratings; (050.1965) Diffractive lenses; (340.7480) X-rays, soft x-rays, extreme ultraviolet (EUV).

http://dx.doi.org/10.1364/AO.55.007218

1. INTRODUCTION

A Dammann grating (DG), which is also considered as a holographic grating [1], is in essence a binary-phase grating whose trip-point phases are optimized to generate some equal-intensity spots at different diffraction orders [2–5]. Generally, the traditional DG has been applied to produce either one-dimensional (1D) or two-dimensional (2D) array illumination in a single far-field plane [2–5], whose functionality can be usually completed by use of a positive lens. With further research, multiple equal-intensity spots on-axis have been generated by means of a Dammann zone plate (DZP) [6]. Recently, based on the above fundamental technologies, three-dimensional (3D) array spots were successfully realized by a combination of DZP and 2D-array illumination DG [7]. Array illuminators have been widely applied in optical couplers [8,9], beam splitters [10], lithography [11], profilometry [12], generation of special fields [13,14], laser systems [15,16], and so on.

From the previous work of predecessors, we know that DG has two significant characteristics: it is a phase-only diffractive optical element (DOE), and only works in the far field. The former characteristic is not suitable for array illumination in the x-ray and the EUV regions due to the strong absorption, and the latter restricts its application field to a certain extent. By contrast, Fresnel zone plates (FZP) can focus the light into a pronounced spot from the x-ray to the EUV region. Unfortunately, using traditional FZP it is difficult to generate array illumination. Here we extend the traditional FZP into a Fresnel–Dammann zone plate (FDZP), which is considered as a FZP with Dammann modulation. Different from the binary-phase DG for array illumination, FDZP can also be an amplitude modulation. In this case, FDZP not only has the function of traditional FZP, but also produces 3D array spots. Array illumination can be applied for laser micromachining, optical tweezers, beam shaping and laser demonstration, array focusing and imaging, etc.

2. FRESNEL–DAMMANN ZONE PLATE (FDZP)

A. Principle

In this section, we will take 2nd-order 3-circle illumination as an example, and investigate the difference between DG and FDZP in detail. Figure 1 shows the optical path of circular Dammann grating (CDG) and FDZP. CDG is a binary-phase grating. Figure 2 illustrates the concrete structure of them. In Fig 2(a), the black is the pi phase, while the white is the zero phase. Either zero or pi phase is a simply connected region. For FDZP in Fig 2(b), the fuchsia, green, and red denote the odd zones, and the rest are even zones. Note that the fuchsia and yellow area is the innermost region, the green and blue area is the middle region, and the red and blue-green area is the outmost region. The above three regions completely coincide with those of CDG, which means that FDZP and the corresponding CDG share the same normalized transitional radii. Now we take into account the amplitude-only FDZP, wherein the even (or yellow) zones are in use in the innermost region, the odd

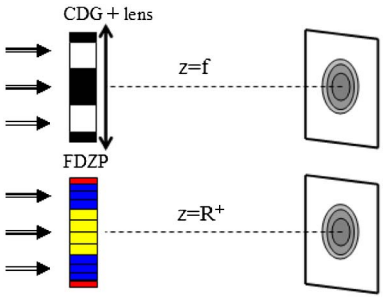

Fig. 1. 2nd-order 3-circle illumination generated by CDG or FDZP.

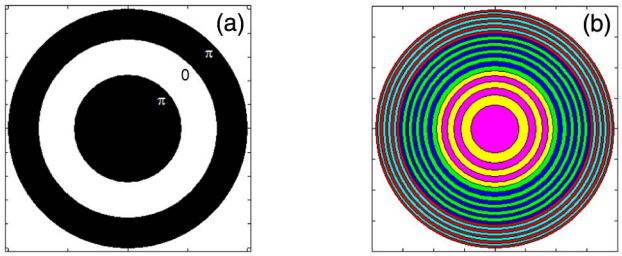

Fig. 2. Schematic of (a) CDG with binary phase, (b) FDZP with opaque and transparent zones.

(green) zones are in use in the middle region, and the even (blue-green) zones are in use in the outermost region. Different from the binary phase of CDG, the phase of FDZP is continuous from zero to pi for odd zones, while the even zones vary from negative π to zero. Obviously, the value of the phase from zero to π is located at the upper-half-plane in the complex plane, and has the same optical effect to the zero phases of CDG. As for the other case, it is vice versa.

B. Diffraction Model

Based on the Fresnel–Kirchhoff diffraction theory, we can get the diffracted field of a single Fresnel zone, that is

$$U_n(S_2) = \iint_{n\text{th-zone}} E_n(S_1) \frac{e^{ik(p+q)}}{i\lambda pq} \frac{\cos\theta_q - \cos\theta_p}{2} \mathrm{d}S_1, \quad (1)$$

where p is the distance from the light source to the FDZP, and q is the diffracted distance between the FDZP and the observed plane. θ_p is the incident angle, and θ_q is the diffraction angle. S_1 denotes the coordinates on the planar FDZP, S_2 denotes the observed plane, and E_n denotes the light field of the corresponding S_1 area on the nth-zone of the planar FDZP.

According to the linear superposition principle, the total diffracted field distribution $U(S_2)$ at the observed plane is the simple sum of the individual diffracted fields. So the total diffracted fields $U(S_2)$ can be written as

$$U(S_2) = \sum_{n=1}^{N} U_n(S_2). \quad (2)$$

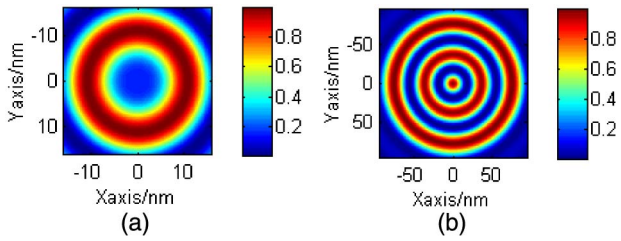

Fig. 3. Array illumination on the focal plane located at 250 μm (a) 1st-order, 2-circle dark-hollow, (b) 2nd-order, 3-circle.

C. Array Illumination of Amplitude-only FDZP

Due to the too-short wavelength of x-rays or EUVs, it is nearly impossible to operate the wavefront by phase-only CDG. In contrast, FDZP can be constructed in the form of amplitude modulation, so it has no difficulty in producing array illumination in the x-ray region.

The wavelength λ_0 is 4.2 nm, which is in the water window. FDZP has 300 zones totally, and the optical path difference scaling factor (OPDSF) K_0 is equal to 0.5, and its focal length f_0 is 250 μm. Accordingly, the outmost zone width is 29.66 nm. Taking the planar wave incidence into account, in case (1), the odd zones are in use on condition that the radius is less than 0.715 times the radius of the device; otherwise, the even zones are in use. In case (2), the odd zones are in use on condition that the radius is less than 0.242 times or larger than 0.662 times the radius of the device; otherwise, the even zones are in use. The first FDZP can generate 1st-order 2-circle dark-hollow illumination, while the second FDZP can generate 2nd-order 3-circle illumination, as shown in Fig. 3.

3. EXTENDED APPLICATION OF FDZP

A. Multi-spots on Axis

Traditional DG can generate array spots in a single plane. In comparison, DZP can generate multi-spots on the axis. The basic concept is that some fine structures are introduced into the DG in order to obtain a series of phase reversal points in each binary-phase region. These characteristics result in all the spots being located at some defocusing planes; therefore, the distance between any two axial spots is at the micro-scale.

Compared with DZP, FDZP can overcome these drawbacks, and generate the multi-spots on the axis, which has axial spacing in the macro-scale. References [17,18] had taken use of a diffractive optical lever to increase the number of axis spots by optical path difference scaling factor (OPDSF). We find that when the number of zones of FDZP goes up to some extent, each spot will be split into so many parts that even a single spot has multiple peaks. On the other hand, from the definition of the Fresnel zone $r_n^2 \approx 2nK\lambda f$ we know that the OPDSF and the wavelength have the same status to affect the number of axial spots. That is to say, the increase of OPDSF is equivalent to the decrease of incident wavelength, and vice versa. So, we can recur to the shortened wavelength to realize multi-spots on the axis. Note that in order to get more than one axial spot, their optical structures are different, since the optical path difference (OPD) between two adjacent zones of the former method equals $K\lambda$ where K is not equal to 0.5, but the latter

is essentially a traditional FZP. Different optical structures mean they have different transmission functions. The benefit of the latter method is that it is effective at preventing the split of axial spots.

To understand the concept well, we present a concrete example. A reference FZP, which is in essence a FDZP without Dammann modulation, has been constructed with 1022 zones totally, a focal length 250 μm, and the designed wavelength is 4.2 nm. The outmost zone width is 16.13 nm. If the value of the OPDSF is set as 1.32, the corresponding outmost zone width is 26.49 nm. In this case we can obtain two axial spots, as shown in Fig. 4(a). To make the contrast even more remarkable, we simultaneously give the enlarged inset which corresponds to the first focal spot. In fact, although the second axial spot is not discussed, it is also split. Figure 4(b) shows that when a plane wave with a wavelength of 3.18 nm illuminates the reference FZP, we also get two axial spots. The difference between them is that the two spots are all not split this time.

Then, still taking FDZP without Dammann modulation as an example, the structure parameters are the same as those in Fig. 3. Naturally, it has degenerated into a traditional FZP. When a planar wave with wavelength 1.91 nm is incident on the FZP, two axial spots are generated, and are located at 183.1 μm and 550.6 μm, respectively. If the incident wavelength is 1.0 nm, there are three axial spots which are located at 209.9 μm, 350.2 μm, and 1051.0 μm, respectively. The two results are shown in Fig. 5. In addition, each inset denotes the transverse intensity distribution on its own focal plane. Note that the ratio of the two FWHMs (full width at half-maximums) are equal to that of their focal length. We can further present the position formula of the axial spots on condition that the OPDSF is equal to 0.5, that is,

$$F_n = \frac{\lambda_0 f_0}{(2n+1)\lambda}, \qquad n \in N, F_n < \ldots < F_0. \tag{3}$$

Obviously, the distance between any pair of spots is far away from the designed focal plane. By contrast, the multi-spots on the axis produced by DZP are all distributed near the focal plane.

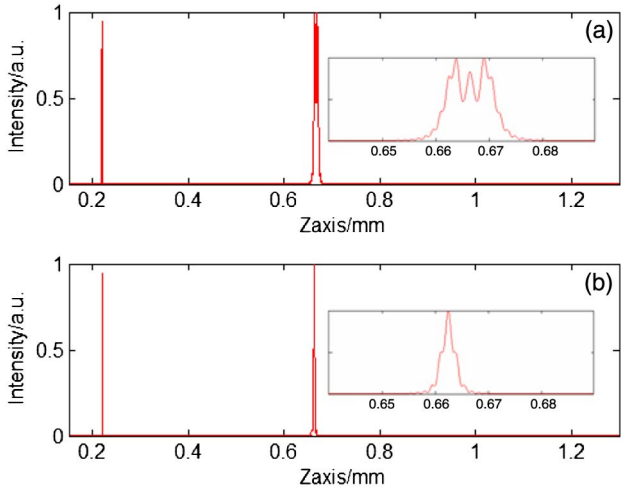

Fig. 4. Two axial spots generated by the reference FZP with different optical structures, (a) $K = 2.64K_0$, (b) $\lambda = \lambda_0/1.32$.

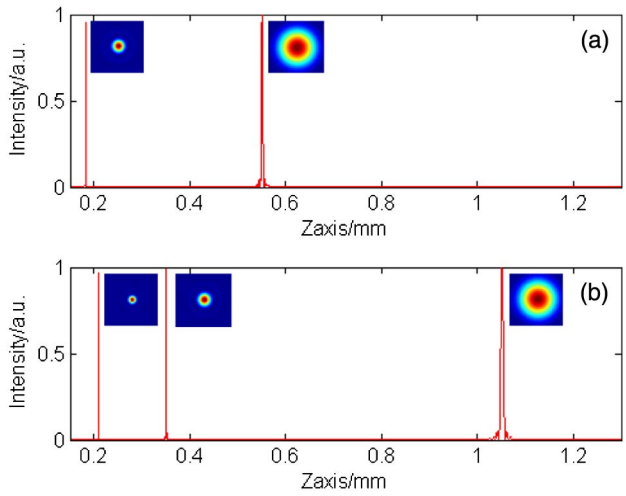

Fig. 5. Multi-spots on the axis generated by FDZP without Dammann modulation, (a) $\lambda = 1.91$ nm, (b) $\lambda = 1.00$ nm.

B. Multi-layer, Multi-circle Illumination

As we know, the combination of CDG and DZP can generate 3D array spots. Likewise, all the spots seem to be the same size because they are located at some defocusing planes with small spacing. As for FDZPs, they can produce array spots with large spacing, which results in a different transverse resolution on the different position. Figure 6 illustrates the schematic described above.

In Section 2, we have separately obtained 2-circle and 3-circle illumination in a single plane. Similarly, multi-layer array illumination with controllable and adjustable characteristics can be easily produced by shortened wavelength incidence. For the same FDZP calculated in Fig. 3(a), when the incident wavelength is reduced to 45.45% relative to the reference wavelength, 2-layer, 2-circle illumination has been successfully generated. The two focal planes are located at 183.1 μm and 550.6 μm, respectively. Figure 7 indicates the corresponding simulation results. If we adopt the same structure in Fig. 3(b), meanwhile, and reduce the incident wavelength to 23.81%, we finally get 3-layer, 2nd-order, 3-circle illumination. The three focal planes, as shown in Fig. 8, are located at 209.9 μm, 350.2 μm, and 1051.0 μm, respectively.

Based on the above discussion, we can take the following steps to construct a FDZP in order to realize more than one

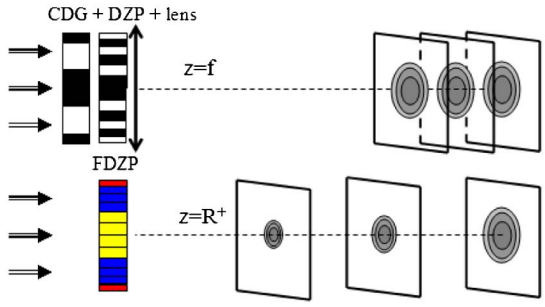

Fig. 6. Schematic of 3D array spots generated by a combination of CDG and DZP or a single FDZP.

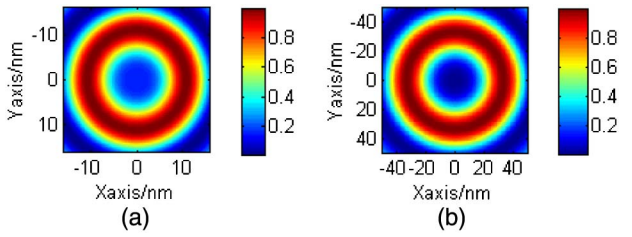

Fig. 7. 2-layer, 1st-order, 2-circle dark-hollow illumination generated by a single FDZP, (a) $z = 183.1$ μm, (b) $z = 550.6$ μm.

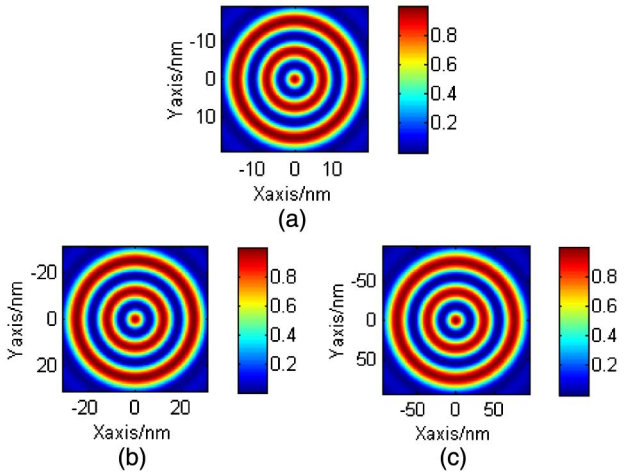

Fig. 8. 3-layer, 2nd-order, 3-circle illumination generated by a single FDZP, (a) $z = 209.9$ μm, (b) $z = 350.2$ μm, (c) $z = 1051.0$ μm.

layer spot: (1) to set the operating wavelength; (2) to design a FZP according to a virtual wavelength which is much longer than the operation wavelength; (3) to choose the suitable Fresnel zones to replace the simply connected region of optimized DG. However, the resolution is still determined by the smallest feature size of the transparent region. It is important to add that, if we want to get multiple spots with controllable and adjustable characteristics, we can adopt other principles, such as the aperiodic Greek-ladder or the generalized Fibonacci structure [17–19].

4. CONCLUSION

Traditional phase-only DG can realize multiple spots in the far field. But the distance between any pair of layers is usually at the micro-scale. Due to the strong absorption, it cannot be applied to the focusing of x-rays and EUVs. We have extended the traditional FZP into FDZP. The major difference among them is that each simply connected region of DG is replaced by discrete Fresnel zones. This way, FDZP can be constructed in the form of amplitude modulation, and can be used for focusing at short wavelength regions. In addition, the distance between any pair of layers comes up to the macro-scale. Of course, for the visible wavelengths, if the Fresnel zones not in use are reversed by relief microstructures, the diffraction efficiency of FDZP can be improved greatly. This kind of diffractive optical element may have many applications in multiple image fusion and laser optics.

Funding. National Natural Science Foundation of China (NSFC) (61205212, 61505228).

REFERENCES

1. H. Dammann and K. Görtler, "High-efficiency in-line multiple imaging by means of multiple phase holograms," Opt. Commun. **3**, 312–315 (1971).
2. H. Dammann and E. Koltz, "Coherent optical generation and inspection of two-dimensional periodic structures," Opt. Acta **24**, 505–515 (1977).
3. C. Zhou and L. Liu, "Numerical study of Dammann array illuminators," Appl. Opt. **34**, 5961–5969 (1995).
4. J. Jia, C. Zhou, and L. Liu, "Circular Dammann grating and its applications," Proc. SPIE **4923**, 119–126 (2002).
5. C. Zhou, J. Jia, and L. Liu, "Circular Dammann grating," Opt. Lett. **28**, 2174–2176 (2003).
6. J. Yu, C. Zhou, W. Jia, J. Wu, and Y. Lu, "Manifestation of Gouy phase anomaly in a coaxial focus array generated by a Dammann zone plate," J. Opt. Soc. Am. A **31**, 1059–1066 (2014).
7. J. Yu, C. Zhou, W. Jia, W. Cao, S. Wang, J. Ma, and H. Cao, "Three-dimensional Dammann array," Appl. Opt. **51**, 1619–1630 (2012).
8. C. Di, C. Zhou, and H. Ru, "Dynamic optical coupler using a Dammann grating," Proc. SPIE **5623**, 81–87 (2005).
9. C. Di and C. Zhou, "Dynamic optical coupled system employing even-numbered Dammann gratings," Appl. Opt. **45**, 1993–2000 (2006).
10. G. Li, C. Zhou, and E. Dai, "Splitting femtosecond laser pulses by using a Dammann grating," Proc. SPIE **5642**, 412–417 (2005).
11. W. Wang, C. Zhou, and W. Jia, "High-fidelity replication of Dammann gratings using soft lithography," Appl. Opt. **47**, 1427–1429 (2008).
12. J. Zhang, C. Zhou, and X. Wang, "Three-dimensional profilometry using a Dammann grating," Appl. Opt. **48**, 3709–3715 (2009).
13. R. V. Vinu, M. K. Sharma, R. K. Singh, and P. Senthilkumaran, "Generation of spatial coherence comb using Dammann grating," Opt. Lett. **39**, 2407–2410 (2014).
14. J. Yu, C. Zhou, J. Wu, L. Zhu, W. Jia, Y. Lu, and S. Li, "Standing quasi-diffraction-free beams generated by circular Dammann gratings under high-order radially polarized Laguerre-Gaussian incidence," Opt. Commun. **335**, 102–107 (2015).
15. B. Li, E. Dai, A. Yan, X. Lv, Y. Zhi, J. Sun, and L. Liu, "Simulations of conjugate Dammann grating based 2D coherent solid-state laser array combination," Opt. Commun. **290**, 126–131 (2013).
16. J. Li, Y. Yao, J. Yu, K. Xia, and C. Zhou, "Efficient vortex laser with annular pumping formed by circle Dammann grating," IEEE Photon. Technol. Lett. **28**, 473–476 (2016).
17. J. Zhang, "Three-dimensional array diffraction-limited foci from Greek ladders to generalized Fibonacci sequences," Opt. Express **23**, 30308–30317 (2015).
18. J. Ke and J. Zhang, "Generalized Fibonacci photon sieves," Appl. Opt. **54**, 7278–7283 (2015).
19. J. Ke and J. Zhang, "Focusing properties of phase-only generalized Fibonacci photon sieves," Opt. Commun. **368**, 34–38 (2016).